Electronic Spectra of Some Methyl Substituted Benzenes in a Rare-Gas Solid

BENJAMIN KATZ
Department of Chemistry, Tel-Aviv University, Tel-Aviv, Israel
AND
MALKA BRITH
Department of Chemistry, Bar-Ilan University, Ramat Gan, Israel
AND
BENJAMIN SHARF AND JOSHUA JORTNER
Department of Chemistry, Tel-Aviv University, Tel-Aviv, Israel
(Received 8 June 1970)

In this paper we present the results of an experimental study of the absorption spectrum of toluene, toluene-d_8, *para*-xylene, and *meta*-xylene in solid krypton in the spectral region 2800–1800 Å. Our main results are:

(a) The absorption spectrum of the first (2700 Å) $\pi \rightarrow \pi^*$ transition is very sharp for all these matrix isolated molecules and resembles in detail the gas-phase spectrum.
(b) The observed vibrational structure of the second (2200 Å) $\pi \rightarrow \pi^*$ transition is consistent with the $^1A_{1g} \rightarrow {}^1B_{1u}$ assignment for this transition in the benzene molecule.
(c) The vibrational structure of the third (1850 Å) $\pi \rightarrow \pi^*$ transition was resolved. An electronic splitting of 350 cm^{-1} was observed in the third excited state of *para*-xylene, which results from lifting of the degeneracy of the corresponding $^1E_{1u}$ state of the benzene molecule.

I. INTRODUCTION

In spite of extensive experimental and theoretical work on the excited electronic states of the benzene molecule,[1] some open questions remained concerning the assignment of the higher $\pi \rightarrow \pi^*$ transitions in this system. In a recent spectroscopic study[2] of the benzene molecule in low-temperature rare-gas matrices we have demonstrated that the vibrational structure of the second spin allowed $\pi \rightarrow \pi^*$ transition is consistent with the $^1A_{1g} \rightarrow {}^1B_{1u}$ rather than with the $^1E_{2g}$ assignment for this excitation. This conclusion is at variance with recent energy levels calculations within the framework of SCFCI π-electron theory[3] which currently seem to support the $^1A_{1g} \rightarrow {}^1E_{2g}$ assignment. It should, however, be pointed out that in our work on the benzene molecule[2] in low-temperature rare-gas solids we failed to observe the crystal field induced 0–0 transition and further work on this problem seems to be desirable. Further support for the $^1B_{1u}$ assignment of the second singlet excited state of the benzene molecule can be obtained from symmetry breaking effects resulting in the reduction of molecular symmetry by chemical substitution. Thus, in methylated benzenes, both pure electronic and the vibronically induced components may be observed. On the basis of simple group theoretical arguments (Table I) one can conclude that for C_{2v} symmetry (e.g., toluene or *meta*-xylene) the 0–0 component is allowed for both states of methylated benzenes having $^1E_{2g}$ and $^1B_{1u}$ parentage of the states of the benzene molecule. On the other hand, for D_{2h} symmetry (e.g., *para*-xylene) the pure electronic transition is allowed for the $^1B_{1u}$ state and forbidden for the configuration of $^1E_{2g}$ parentage.

Complications arise in the interpretation of high intravalence excitations of large molecules. In contrast to the lowest spin allowed excitation of the benzene molecule and of substituted benzenes in the gas phase which reveal sharp absorption bands (where diffuseness of the spectral lines can be assigned to "trivial" broadening mechanisms[4]), the higher excited states are extremely diffuse.[5] Trivial mechanisms[4] such as the appearance of overlapping hot bands and sequence congestion cannot be blamed for this diffuseness, which mainly arises from intramolecular electronic relaxation.[6] This diffuseness persists in low-temperature matrices. Low-temperature studies of the second and third $\pi \rightarrow \pi^*$ transitions of methylated benzenes in hydrocarbon glasses[7] led to some information on the vibrational structure and matrix shifts for these transitions. However, the hydrocarbon glasses employed by Potts (3-methylpentane and isopentane) do not apparently provide a proper Shpolskii[8] matrix for the benzene molecule and its derivatives and exhibit appreciable phonon broadening. We have attempted to study those transitions of methyl benzenes in rare-gas solids where previous work[2] revealed well-defined (although broadened) vibronic bands in the second and third spin allowed transition of the benzene molecule. A further complication introducd by the use of rare-gas hosts involves the appearance of fine structure assigned to different trapping sites. We have recently demonstrated[2] that the use of annealed rare-gas solids (prepared by deposition at 40°K) leads to a considerable reduction of the fine structure assigned to different trapping sites. This technique facilitates the experimental observation and the interpretation of the higher excited transitions of benzene and its derivatives. As the appearance of fine structure in the 2600-Å transition of benzene in rare-gas solids was always observed simultaneously with the fine

structure in the higher $\pi \rightarrow \pi^*$ transitions, we found it necessary to study also the 2600-Å transition of methyl substituted benzenes in this medium. The information on the vibrational structure obtained for the lowest transition in rare-gas solids concurs with previous gas-phase studies and could then be applied for the interpretation of the vibrational structure of the second excited state.

To summarize, we assess that line broadening in the higher excited states of large molecules such as methylated benzenes in low-temperature rare-gas solids may arise mainly from the following factors:

(a) Coupling with lattice vibrations.
(b) Intramolecular radiationless decay.
(c) Vibrational relaxation.
(d) Unresolved vibrational components.
(e) Site splittings and distribution of different trapping sites.

From the study of the 2600-Å absorption system of benzene we can conclude that effects (a) and (c) are relatively small (leading to a contribution to line broadening ~ 10 cm^{-1}). The apparent linewidths observed for the second and third transition in toluene and *meta*-xylene considerably exceed those previously obtained for the same transitions in benzene. The theory of nonradiative decay processes[4,6] is not sufficiently advanced at present to provide a proper interpretation for the difference in nonradiative decay probabilities of different methyl substituted benzenes. We just had to rely on experimental observation of linewidths with respect to the proper choice of a system. The most conclusive data in this respect were obtained for the *p*-xylene molecule.

The primary goal of the present work has been to obtain detailed information on the vibrational structure of the second excited singlet state of methyl substituted benzenes. Another interesting problem involves the splitting of the electronic degeneracy by chemical substitution in the third $\pi \rightarrow \pi^*$ excited state of these systems which is of $^1E_{1u}$ parentage (see Table I). The $\pi \rightarrow \pi^*$ $^1E_{1u}$ excited state of the benzene molecule is not Jahn–Teller active as the two degenerate components cannot be (in first order) coupled by one electron perturbation. However, methyl (or other chemical) substitution will lead to the splitting of these energy levels. In the ground state of negative ions of methylated benzenes the pseudo-Jahn–Teller effect was extensively studied.[9] To our knowledge, no experimental evidence for the magnitude of this electronic splitting is available in excited electronic states of substituted benzene.

Finally, an attempt was made to extract some qualitative information from the linewidths of the second and third transitions of methylated benzenes in low-temperature rare-gas matrices concerning nonradiative decay phenomena in these molecular systems.

TABLE I. Correlation table.

D_{6h}	C_{2v}	D_{2h}
B_{2u}	B_1	B_{3u}
B_{1u}	A_1	B_{2u}
E_{2g}	A_1+B_1	A_g+B_{1g}
E_{1u}	A_1+B_1	$B_{2u}+B_{3u}$

II. EXPERIMENTAL PROCEDURES

The gas mixtures at the molar ratio 1:100 were deposited on a cooled LiF window in the temperature range 20–40°K. The spectra were photographed at 20°K. The temperature control device employed was described by Savitsky and Hornig.[10] Liquid hydrogen was used as a refrigerant. The spectra were photographed on a 2-m Eagle mounting grating vacuum spectrograph,[11] with a dispersion of 7.5 A/mm in first order and a resolution of 50 000. A microwave discharge H_2 light source was used. Kodak SWR plates were employed. Microdensitometer tracings of the plates were prepared using a Joyce and Loble recording microdensitometer. The microdensitometer tracings were not corrected for the wavelength variation of source intensity. The frequencies of the absorption bands were measured both from the microdensitometer tracings and directly from the plates. The emission lines of Hg, C, O, and H were used for calibration. In view of the appreciable line broadening in the second and in the third excited states of methylated benzenes all the measurements of the line frequencies for the second and third transitions are accurate within ± 30 cm^{-1}, while level spacings are accurate within ± 50 cm^{-1}.

In some cases, the relative intensities of the fine-structure lines in one band, or relative intensities of the vibronic bands corresponding to a single electronic transition were estimated by a procedure similar to that described in a previous paper.[2]

Toluene, *meta*-xylene, *para*-xylene (Matheson), and deuterotoluene (Merck and Sharp) of both spectrograde and chromatographic grade were used. An extra chromatographic analysis was carried out on *para*-xylene to exclude the possibility of contamination by any other isomer.

III. THE 2650-Å TRANSITION

The experimental results obtained for the first spin allowed transition of toluene, toluene-d_8, *m*-xylene, and *p*-xylene are analyzed in Tables II–VI. The normal vibrational modes are labeled according to the conventional notation as summarized by Herzberg.[12] For further reference the relevant ground state frequencies are summarized in Table II. These data are taken from the work of Pitzer and Scott.[13] Comparison of the low-temperature matrix spectra (Tables III–VI) with previous gas-phase work on toluene,[14] *meta*-xylene,[15] and

TABLE II. Ground state vibrational frequencies for benzene and some methylated benzenes.[a]

Benzene D_h		Toluene C_{2v}		*m*-Xylene C_{2v}		*p*-Xylene D_{2h}	
$\nu_2(a_{1g})$	992	$\nu_2(a_1)$	1002	$\nu_2(a_1)$	998	$\nu_2(a_g)$	826
$\nu_{11}(e_{1g})$	849	$\nu_{11}(b_1)$	730	$\nu_{11}(b_1)$	276	$\nu_{11}(b_{3g})$	813
		$\nu_{11}(a_1)$	842	$\nu_{11}(a_1)$	770	$\nu_{11}(b_{2g})$	811
$\nu_{15}(e_{2g})$	3047	$\nu_{15}(a_1)$	1210	$\nu_{15}(a_1)$	(3047)	$\nu_{15}(a_g)$	1204
		$\nu_{15}(b_1)$	3047	$\nu_{15}(b_1)$	945	$\nu_{15}(b_{1g})$	3047
$\nu_{16}(e_{2g})$	1596	$\nu_{16}(a_1)$	1603	$\nu_{16}(a_1)$	1592	$\nu_{16}(a_g)$	1616
		$\nu_{16}(b_1)$	1586	$\nu_{16}(b_1)$	1613	$\nu_{16}(b_{1g})$	1575
$\nu_{17}(e_{2g})$	1178	$\nu_{17}(a_1)$	1175	$\nu_{17}(a_1)$	1167	$\nu_{17}(a_g)$	1182
		$\nu_{17}(b_1)$	1155	$\nu_{17}(b_1)$	1152	$\nu_{17}(b_{1g})$	313
$\nu_{18}(e_{2g})$	606	$\nu_{18}(a_1)$	521	$\nu_{18}(a_1)$	538	$\nu_{18}(a_g)$	460
		$\nu_{18}(b_1)$	622	$\nu_{18}(b_1)$	514	$\nu_{18}(b_{1g})$	644
$\nu_{13}(e_{1u})$	1485	$\nu_{13}(a_1)$	1483	$\nu_{13}(a_1)$	(1320)	$\nu_{13}(b_{2u})$	1525
		$\nu_{13}(b_1)$	1310	$\nu_{13}(b_1)$	(1470)	$\nu_{13}(b_{3u})$	1450
$\nu_{14}(e_{1u})$	1037	$\nu_{14}(a_1)$	1030	$\nu_{14}(a_1)$	224	$\nu_{14}(b_{2u})$	1030
		$\nu_{14}(b_1)$	340	$\nu_{14}(b_1)$	310	$\nu_{14}(b_{3u})$	(232)
$\nu_6(b_{1u})$	1011	$\nu_6(a_1)$	785	$\nu_6(a_1)$	724	$\nu_6(b_{2u})$	720

[a] Data from Pitzer and Scott.[13] Notation is according to Herzberg.[12] All data in cm^{-1}.

p-xylene,[16] reveals the following features:

(a) The fundamental vibrational frequencies and their relative intensities observed in the solid matrices are in good agreement with the gas-phase data. The present low-temperature data are simpler in this respect as no hot bands are exhibited.

(b) There is a red spectral shift of $\sim$200 cm^{-1} in the krypton matrix relative to the gas-phase data.

The spectra of toluene-h_8 and *p*-xylene are displayed in Figs. 1–3. As in previous work on the benzene molecule in inert matrices,[2,17] we have observed fine structure in the absorption bands of methylated benzenes in a Kr matrix. The spectra of toluene-h_8 and toluene-d_8 are characterized by two fine-structure components of about equal intensity spaced by $\sim$25 cm^{-1} in toluene and $\sim$30 cm^{-1} in toluene-d_8 (see Fig. 1). The spectrum of *p*-xylene is characterized by three fine-structure components (see Fig. 3), the spacing being 20 and 50 cm^{-1} from the low-energy component. Similar fine structure characterized by splitting of 80 cm^{-1} in the $^1B_{2u}$ state was previously observed in benzene in rate-gas matrices.[2,17] This structure is attributed to different trapping sites in the matrix. The assignment of the fine structure to different trapping sites is strongly supported by the observation of this structure in the 0–0 band. In previous work,[2] we have found that the deposition of benzene–

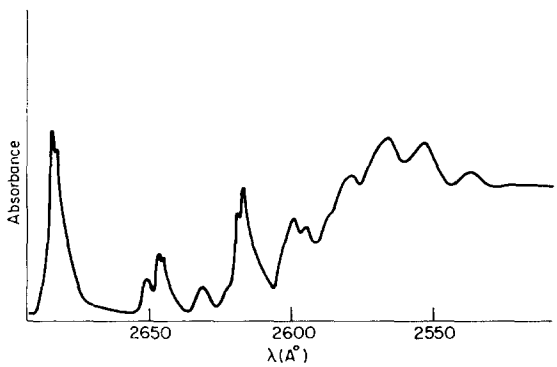

FIG. 1. The 2650-Å absorption system of toluene-h_8 in solid krypton. Because of the low resolution of the microdensitometer, the fine structure is not well resolved, while it is well resolved in the photographic plates. In view of the diffuseness of the overtones and the combination bands, the fine structure is smeared out. The gas mixture was deposited at 40°K and photographed at 20°K.

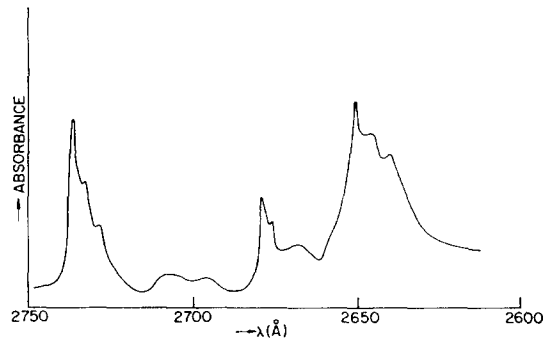

FIG. 2. A high-resolution microdensitometer tracing of the 0–0 band of the 2650-Å absorption system of *p*-xylene in solid krypton. The sample was deposited at 40°K and photographed at 20°K.

TABLE III. Analysis of the absorption spectrum of toluene-h_8 in solid krypton at 20°K; transition $^1A_1 \rightarrow {}^1B_1$ ($^1A_{1g} \rightarrow {}^1B_{2u}$ in benzene).

Wavelength (Å)	Frequency (cm^{-1})	Intensity	$\nu - \nu_{00}$ (cm^{-1})	Vibrational assignment	Gas-phase frequency[a] (cm^{-1})
2684.0	37 258	vvs	0	0-0	37 477
2682.5	37 279	vvs		0-0+21 cm^{-1}	
2668.5	37 474	vvw(dif)[b]	210	ghost	
2651.8	37 710	w-m	452	$0\text{-}0+\nu_{18}(a_1)$	456(m)
2649.6	37 742	w-m	484	$0\text{-}0+\nu_{18}(a_1)+32$ cm^{-1}	
2646.2	37 790	s	532	$0\text{-}0+\nu_{18}(b_1)$	528(s)
2644.3	37 817	s	559	$0\text{-}0+\nu_{18}(b_1)+27$ cm^{-1}	
2630.9	38 010	w-m(dif)	750	$0\text{-}0+\nu_6(a_1)$	751(m)
2618.4	38 191	vs	933	$0\text{-}0+\nu_2(a_1)$	932(vs)
2616.5	38 219	vs	961	$0\text{-}0+\nu_{14}(a_1)$; $0\text{-}0+\nu_2(a_1)+28$ cm^{-1}	964(s)
2614.4	38 250	vs	992	$0\text{-}0+\nu_{14}(a_1)+31$ cm^{-1}	
2601.7	38 440	m	1180	$0\text{-}0+\nu_{15}(a_1)$	1 189(ms)
2599.4	38 470	m	1221	$0\text{-}0+\nu_{15}(a_1)+41$ cm^{-1}	
2594.2	38 550	w(dif)	1290±30	$0\text{-}0+\nu_6(a_1)+\nu_{18}(b_1)$	
2586.7	38 660	vw(dif)	1400±30	$0\text{-}0+\nu_2(a_1)+\nu_{18}(a_1)$	
2583.0	38 715	m	1457	$0\text{-}0+\nu_2(a_1)+\nu_{18}(b_1)$	
2580.5	38 752	m+	1494	$0\text{-}0+\nu_2(a_1)+\nu_{18}(b_1)+30$ cm^{-1}; $0\text{-}0+\nu_{14}(a_1)+\nu_{18}(b_1)$	
2578.5	38 782	m	1524	$0\text{-}0+\nu_{14}(a_1)+\nu_{18}(b_1)+30$ cm^{-1}	
2565.5	38 980	dif	1720±30	$0\text{-}0+\nu_2(a_1)+\nu_6(a_1)$	
2553.8	39 167	w	1909	$0\text{-}0+2\nu_2(a_1)$	
2552.3	39 180	w	1922	$0\text{-}0+2\nu_2(a_1)+\nu_{14}(a_1)$; $0\text{-}0+2\nu_2(a_1)+23$ cm^{-1}	
2550.1	39 214	w	1956	$0\text{-}0+2\nu_{14}(a_1)$; $0\text{-}0+2\nu_2(a_1)+\nu_{14}(a_1)+33$ cm^{-1}	
2538.1	39 400	w	2140±30	$0\text{-}0+\nu_2(a_1)+\nu_{15}(a_1)$	
2503.7	39 940	vw	2680±30	$0\text{-}0+\nu_2(a_1)+\nu_{14}(a_1)+\nu_6(a_1)$	
2488.7	40 180	vw(dif)	2920±30	$0\text{-}0+2\nu_{15}(a_1)+\nu_{18}(b_1)$	
2477.5	40 360	vw(dif)	3100±30	$0\text{-}0+\nu_2(a_1)+\nu_{14}(a_1)+\nu_{15}(a_1)$	
2435.0	41 070	vw	3810±30	$0\text{-}0+2\nu_2(a_1)+2\nu_{14}(a_1)$	

[a] The number in this column refers to the location of the 0-0 line in the gas phase, while the other data represent the gas-phase vibrational frequencies (see Ref. 14).

[b] (dif) refers to a diffuse band.

rare-gas mixtures at 40°K followed by measurements at 20°K led to an appreciable reduction in the fine structure assigned to different trapping sites, while deposition of C_6D_6/Kr mixtures at 40°K still led to appreciable contributions from different sites. As in the case of deuterated benzene[2] we have now found that the deposition of toluene at 20 and at 40°K results in a similar intensity pattern for the different trapping sites, which are characterized by about the same intensity. In the case of *m*-xylene, deposition was carried out only at 20°K. The bands are more diffuse than in toluene and in *p*-xylene. The structure of the bands consists of a narrow line (~20 cm^{-1} for the band 0-0) followed by a rather broad "shadow" (~160 cm^{-1} wide) of weaker intensity. In the case of *p*-xylene three different trapping sites were observed. "High-temperature" (40°K) deposition led to a considerable enhancement of one of these components, the relative intensity of these lines in the 0-0 transition of *p*-xylene was found to be 50:5:1 (see Fig. 3).

IV. THE 2200-Å TRANSITION

The absorption spectra recorded for the second spin allowed transition of toluene, toluene-d_8, and *m*-xylene in a krypton matrix (Fig. 4) are very diffuse. The analysis of these spectra (Tables VII–IX) reveals a totally symmetric $\nu_2(a_1)$ progression built on the pure electronic origin. In addition, the false origin corresponding to the ν_{18} vibration could also be identified. [Strictly speaking, this mode corresponds to a totally symmetric vibration $\nu_{18}(a_1)$ and the false origin $\nu_{18}(b_1)$.] In toluene-h_8 and toluene-d_8 two site-split components were observed having about the same intensity and appreciably overlapping each other. In view of the appreciable widths of the vibronic components no further information could be extracted from these spectra.

The absorption spectrum of *para*-xylene (Fig. 5) reveals well-resolved lines which are amenable to detailed analysis. Only the lines corresponding to the

TABLE IV. Analysis of the absorption spectrum of toluene-d_8 in solid krypton at 20°K; transition $^1A_1 \rightarrow {}^1B_1$ ($^1A_{1g} \rightarrow {}^1B_{2u}$ in benzene).

Wavelength (Å)	Frequency (cm^{-1})	Intensity	$\nu - \nu_{00}$ (cm^{-1})	Vibrational assignment
2671.0	37 439	vs		0-0
2668.8	37 470	vs	31	0-0+31 cm^{-1}
2640.6	37 870	m	431	0-0+$\nu_{18}(a_1)$
2638.9	37 895	m	456	0-0+$\nu_{18}(a_1)$+25 cm^{-1}
2634.4	37 959	s	520	0-0+$\nu_{18}(b_1)$
2621.7	38 143	vw	704	0-0+$\nu_6(a_1)$
2614.3	38 251	w-m	812	0-0+$\nu_{14}(a_1)$[a]
2606.8	38 361	vs	922	0-0+$\nu_2(a_1)$
2604.6	38 394	vs	955	0-0+$\nu_2(a_1)$+33 cm^{-1}
2588.1	38 638	w(dif)	1200±40	0-0+$\nu_{15}(a_1)$
2577.7	38 794	w(dif)	1355±40	0-0+$\nu_2(a_1)+\nu_{18}(a_1)$
2573.2	38 862	w	1423	0-0+$\nu_2(a_1)+\nu_{18}(b_1)$
2570.2	38 907	w	1468	0-0+$\nu_2(a_1)+\nu_{18}(b_1)$+45 cm^{-1}
2562.2	39 029	vw	1590±30	0-0+$\nu_2(a_1)+\nu_6(a_1)$
2553.0	39 170	vw	1730±30	0-0+$\nu_2(a_1)+\nu_{14}(a_1)$
2543.3	39 319	w	1880±30	0-0+$2\nu_2(a_1)$

[a] The energy of this vibration reduces from 964 cm^{-1} in toluene-h_8 to 812 cm^{-1} in toluene-d_8. This appreciable reduction is expected since ν_{14} is a H (||) vibration.

prominent trapping site were observed. Several totally symmetric progressions could be identified (Table X) consisting of the $\nu_2(a_g) \simeq 750$ cm^{-1} and $\nu_{15}(a_g) \simeq 1200$ cm^{-1} and their combinations. The $\nu_{16}(a_g) \simeq 1500$-$cm^{-1}$ vibration could not be conclusively identified as it overlaps the 0-0+$2\nu_2(a_g)$ band. The false origin $\nu_{18}(b_{1g}) = 500$ cm^{-1} was observed. From the comparison with the 2650-Å system the corresponding $\nu_{18}(a_g) \simeq$ 360-cm^{-1} component is probably much weaker in intensity and therefore could not be detected. The observed vibrational structure is inconsistent with Albrecht's theoretical predictions concerning the $^1A_{1g} \rightarrow {}^1E_{2g}$ transition in a model system for p-xylene.[18] In this case, the 0-0 line is forbidden in D_{2h} symmetry and the "false" vibronically induced origins correspond to vibrations of b_{2u} and b_{3u} symmetry. Albrecht's model calculations[18] for the $^1A_{1g} \rightarrow {}^1E_{2g}$ transitions suggest the appearance of

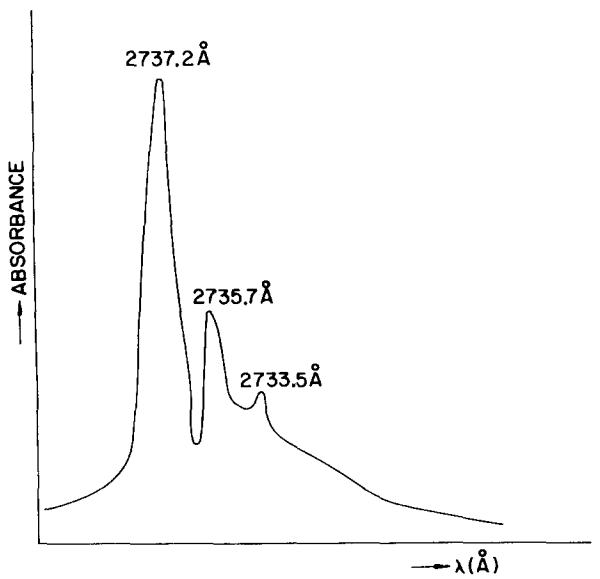

FIG. 3. Part of the absorption spectrum of the 2650-Å transition of p-xylene in solid krypton. Because of low resolution of the microdensitometer, the fine structure is not very well resolved. Sample was deposited at 40°K and photographed at 20°K.

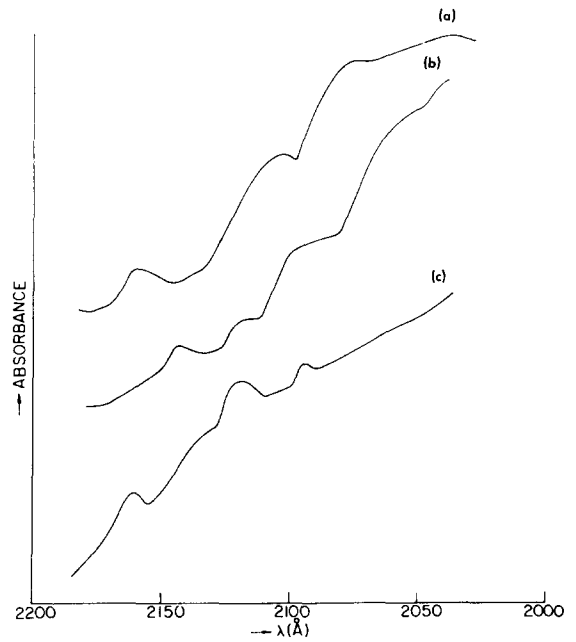

FIG. 4. The absorption spectra corresponding to the 2200-Å transition of several methylated benzenes in solid krypton. (a) Toluene-h_8, deposition at 40°K and measurement at 20°K. (b) Toluene-d_8, deposition and measurement at 20°K. (c) m-Xylene, deposition and measurement at 20°K.

TABLE V. Analysis of the absorption spectrum of *m*-xylene in solid krypton at 20°K; transition $^1A_1 \rightarrow {}^1B_1$ ($^1A_{1g} \rightarrow {}^1B_{2u}$ in benzene). Only the lines of the prominent site are given in the table.

Wavelength (Å)	Frequency (cm^{-1})	Intensity	$\nu-\nu_{00}$ (cm^{-1})	Vibrational assignment	Gas-phase frequency[a] (cm^{-1})
2724	36 710	vs	0	0–0	36 955
2690	37 170	w	460	$0–0+\nu_{18}$	470(s)[b]
2673	37 410	vw	700		675(w), 735(vw)
2654	37 680	s	970	$0–0+\nu_2(a_1)$	965(vs)
2606	38 370	vw	1660	$0–0+\nu_2(a_1)+700$	
2589	38 630	w	1920	$0–0+2\nu_2(a_1)$	

[a] First number corresponds to the gas-phase 0–0 transition, while the other data refer to the excited state gas-phase frequencies (see Ref. 15).

[b] The ν_{18} bands corresponding to the ground state vibrations 515 and 536 cm^{-1} are assumed by Sponer and Cooper (Ref. 15) to be indistinguishable.

at least four false origins of comparable intensity, spaced by ~300, ~1100, and ~1200 cm^{-1} from the lowest false origin. The observed vibrational structure and intensity pattern (Table X) is entirely different. Finally, we should notice the close correspondence between the vibrational structure of the first and second spin allowed transition in *p*-xylene. In particular, one should notice that in *p*-xylene the $\nu_{15}(a_g)$ and the $\nu_2(a_g)$ vibrations appear with about equal intensity. This fact proved essential for the analysis of the 1900-Å transition (see Sec. VI). The $\nu_{15}(a_g)$ vibration is a component of a mode which involves mainly the vibration of the methyl groups. The vibrational energy reduces from $\nu_{15}(e_{2g}) = 3047$ to $\nu_{15}(a_g) = 1204$ cm^{-1} in *p*-xylene (these data correspond to ground state frequencies).

V. ASSIGNMENT OF THE 2200-Å TRANSITION

On the basis of the study of the second spin allowed electronic transition of methylated benzenes, this excitation may now be safely assigned to the $^1A_{1g} \rightarrow {}^1B_{1u}$ parentage in the benzene molecule on the basis of the following arguments:

(1) The vibrational structure of this transition is consistent with this assignment. To amplify this point, we display in Table XI the present data for the excited states vibrational frequencies which are common to all the three $\pi \rightarrow \pi^*$ transitions. The close correspondence between the vibrational modes which appear in the first and in the second transitions of the methylated benzenes strongly supports the assignment for the

TABLE VI. Analysis of the absorption spectrum of *p*-xylene in solid krypton at 20°K, transition $^1A_g \rightarrow {}^1B_{3u}$ ($^1A_{1g} \rightarrow {}^1B_{2u}$ in benzene). Only the lines of the prominent site are given in the table.

Wavelength (Å)	Frequency (cm^{-1})	Intensity	$\nu-\nu_{00}$ (cm^{-1})	Vibrational assignment	Gas-phase frequency[a] (cm^{-1})
2737.2	36 540	vvs	0	0–0	36 733
2709.6	36 900	vw	360	$0–0+\nu_{18}(a_g)$	367(m)
2696.9	37 080	w	540	$0–0+\nu_{18}(b_{1g})$	552(s)
2680.5	37 310	s	770	$0–0+\nu_2(a_g)$	775(vs)
2677.5	37 350	m	810	$0–0+\nu_{11}(b_{2g})$	802(s)[b]
2651.1	37 720	vs	1180	$0–0+\nu_{15}(a_g)$	1 185(vs)
2641.0	37 860	vw	1320	$0–0+\nu_2(a_g)+\nu_{18}(b_{1g})$	
2625.7	38 070	vw	1530	$0–0+2\nu_2(a_g)$	
2623.1	38 110	w	1570	$0–0+\nu_2(a_g)+\nu_{11}(b_{2g})$; $0–0+\nu_{16}(b_{1g})$	
2611.5	38 280	w(dif)	1740	$0–0+\nu_{18}(b_{1g})+\nu_{15}(a_g)$	
2597.7	38 490	ms	1950	$0–0+\nu_2(a_g)+\nu_{15}(a_g)$	
2585.8	38 660	vw(dif)	2120	$0–0+\nu_{18}(b_{1g})+\nu_{16}(b_{1g})$	
2575.4	38 820	vw	2280		
2572.4	38 860	w	2320	$0–0+3\nu_2(a_g)$	
2556.7	39 110	vw	2570	c	
2544.5	39 300	vvw	2760	$0–0+\nu_{15}(a_g)+\nu_{16}(b_{1g})$	

[a] First number in this column refers to the location of the gas-phase 0–0 line, while the other data correspond to the excited state gas-phase frequencies (see Ref. 16).

[b] The assignment of this line is not unambiguous.

[c] Appears also in the gas phase, its assignment is not clear.

TABLE VII. Analysis of the absorption spectrum of toluene-h_8 in solid krypton at 20°K; transition $^1A_1 \rightarrow {}^1A_1$ ($^1A_{1g} \rightarrow {}^1B_{1u}$ in benzene).

Wavelength (Å)	Frequency (cm^{-1})	Intensity	$\nu-\nu_{00}$ (cm^{-1})	Assignment
2160	46 300	vs	0	0–0
2139	46 750	w	450±50	0–0+$\nu_{18}(b_1)$
2117	47 240	vs	950±50	0–0+$\nu_2(a_1)$
2077	48 150	s	1860+50	0–0+$2\nu_2(a_1)$
2036	49 120	m	2830±50	0–0+$3\nu_2(a_1)$
1997	50 070	w	3780±50	0–0+$4\nu_2(a_1)$

TABLE IX. Analysis of the absorption spectrum of *m*-xylene in solid krypton at 20°K; transition $^1A_1 \rightarrow {}^1A_1$ ($^1A_{1g} \rightarrow {}^1B_{1u}$ in benzene).

Wavelength (Å)	Frequency (cm^{-1})	Intensity	$\nu-\nu_{00}$ (cm^{-1})	Vibrational assignment
2162	46 230	s	0	0–0
~2138	46 770	w	~540	0–0+ν_{18}
2112	47 170	s	940	0–0+$\nu_2(a_1)$
2094	47 750	m	1490	0–0+$\nu_2(a_1)+\nu_{18}$
2078	48 130	vw	1870	0–0+$2\nu_2(a_1)$

second transition. Finally, the appearance of the $\nu_{18}(b_{1g})$ vibration in the second transition and the absence of false origins based on the b_{2u} and b_{3u} modes is consistent with $^1A_{1g} \rightarrow {}^1B_{1u}$ rather than with the $^1A_{1g} \rightarrow {}^1E_{2g}$ transition.

(2) The assignment of the lowest vibronic component of this second transition in *para*-xylene to the 0–0 band is conclusive in view of the vibrational analysis of this transition (see Tables X and XI). The observation of the 0–0 line in the 2200-Å transition in a rare-gas solid concurs with the data of Potts.[7] This result again provides a strong supporting evidence for the $^1B_{1u}$ assignment of this transition.

(3) Further support for the $^1B_{1u}$ assignment of this transition is obtained from the pattern of the methyl shifts on the 0–0 line of the 2200-Å transition in toluene and in *p*-xylene. In Table XII, we have assembled the pertinent experimental data concerning these methyl shifts. Bearing in mind that in the benzene molecule the lowest observed vibronic component corresponds to a symmetry forbidden transition, the methyl shifts of the pure electronic origin are

toluene relative to benzene $1300\pm50\ cm^{-1}$,

p-xylene relative to benzene $2300\pm50\ cm^{-1}$.

These methyl shifts are consistent with Petrushka's calculations on the effect of chemical substitution on the center of gravity of the 2200-Å band. These experimental data strongly support the 0–0 assignment in the *p*-xylene 2200-Å absorption. It should, however, be noted that the methyl shift observed for the 2200 Å of *m*-xylene relative to benzene is somewhat too low (see Table XII). Petrushka's calculations[19] indeed predict that the methyl shifts for *m*-xylene and *o*-xylene relative to benzene should be somewhat lower than that for *p*-xylene. Experimental evidence also reveals that in the first electronic transition the methyl shifts for toluene and for *ortho*-xylene are very close (see Table XII).

TABLE VIII. Analysis of the absorption spectrum of toluene-d_8 in solid krypton at 20°K; transition $^1A_1 \rightarrow {}^1A_1$ ($^1A_{1g} \rightarrow {}^1B_{1u}$ in benzene).

Wavelength (Å)	Frequency (cm^{-1})	Intensity	$\nu-\nu_{00}$ (cm^{-1})	Assignment
2144	46 640	vs	0	0–0
2121	47 150	w–m	490±50	0–0+$\nu_{18}(b_1)$
2100	47 620	s(dif)	980±50	0–0+$\nu_2(a_1)$
2065	48 430	s(dif)	1790±50	0–0+$2\nu_2(a_1)$
~2032	49 210	m(dif)	~2570	0–0+$3\nu_2(a_1)$
~1998	50 050	w(dif)	~3400	0–0+$4\nu_2(a_1)$

VI. THE 1900-Å TRANSITION

The absorption spectra corresponding to the third spin allowed transition in toluene-h_8, toluene-d_8, and *m*-xylene (see Fig. 6) are broader and more diffuse than the corresponding transition in the benzene molecule previously reported by us.[2] As in the 2600 and 2200-Å transitions of these molecules the spectra reveal two overlapping site components of about equal intensity. The spectrum of *m*-xylene (Fig. 6) clearly reveals fine structure characterized by site splitting of $180\pm50\ cm^{-1}$ for the first band, which appears as a modulation on the high-energy side of the other vibronic components. The splitting observed in the third electronic transition of

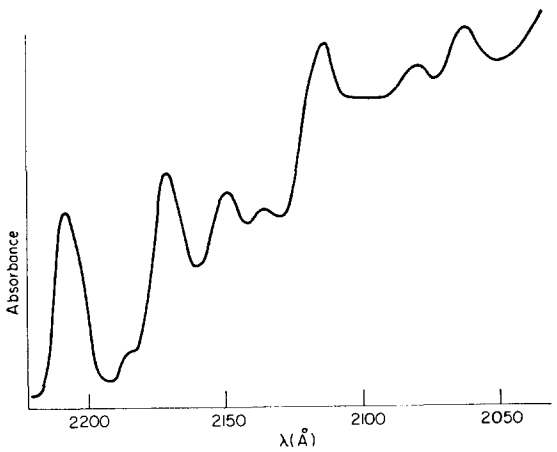

FIG. 5. The 2200-Å absorption system of *p*-xylene in solid Kr, deposition at 40°K and measurement at 20°K.

TABLE X. Analysis of the absorption spectrum of *p*-xylene in solid krypton at 20°K; transition $^1A_{1g} \rightarrow {}^1B_{2u}$ ($^1A_{1g} \rightarrow {}^1B_{1u}$ in benzene).

Wavelength (Å)	Frequency (cm^{-1})	Intensity	Intensity (arbitrary units)	$\nu - \nu_{00}$ (cm^{-1})	Vibrational assignment
2208	45 290	vs	13	0	0–0
2184	45 790	w	~1	500	$0\text{–}0+\nu_{18}(b_{1g})$
2172	46 040	vs	8	750	$0\text{–}0+\nu_2(a_g)$
2152	46 490	s	4	1200	$0\text{–}0+\nu_{15}(a_g)$; $0\text{–}0+\nu_2(a_g)+\nu_{18}(b_{1g})$
2137	46 790	w	1	1500	$0\text{–}0+2\nu_2(a_g)$; $(0\text{–}0+\nu_{16}(b_{1g}, a_g)$
~2125	~47 040	Shoulder		~1750	$0\text{–}0+\nu_{15}(a_g)+\nu_{18}(b_{1g})$
2116	47 240	vs		1950	$0\text{–}0+\nu_{15}(a_g)+\nu_2(a_g)$
2097	47 690	vw		2400	$(0\text{–}0)+2\nu_{15}(a_g)$
2080	48 010	m		2720	$(0\text{–}0)+2\nu_2(a_g)+\nu_{15}(a_g)$; $(0\text{–}0)+\nu_{15}(a_g)+\nu_{16}(b_{1g}, a_g)$
2064	48 450	s		3160	$0\text{–}0+\nu_2(a_g)+2\nu_{15}(a_g)$
~2048	48 830	w		~3540	$0\text{–}0+3\nu_2(a_g)+\nu_{15}(a_g)$
2033	49 180	m		3890	$0\text{–}0+2\nu_2(a_g)+2\nu_{15}(a_g)$
~2014	49 650	w		~4360	$0\text{–}0+\nu_2(a_g)+3\nu_{15}(a_g)$

m-xylene cannot be attributed to a pseudo-Jahn–Teller splitting of the electronic level as multiple trapping sites are observed in the first transition. These spectra of toluene-h_8, toluene-d_8, and *m*-xylene (Tables XIII–XV) reveal just a single totally symmetric vibrational progression built on the 0–0 electronic origin.

The third transition of *p*-xylene reveals some interesting information (see Fig. 7). There is a line located 350 cm^{-1} above the 0–0 transition which is of comparable intensity to the electronic origin. Following these two lines there exists three pairs of bands, each pair separated again by 300–400 cm^{-1} and characterized by about equal intensity (see Table XVI).

The average spacing between the center of gravity of these pairs is about ~750 cm^{-1}. Unlike the corresponding 1900-Å spectrum of benzene[2] or toluene, the *p*-xylene spectrum in this region cannot be assigned to a single vibrational progression even if we invoke the assumption that each band in such a single progression is split by ~350 cm^{-1}. As in both the 2700- and 2200-Å transitions in *p*-xylene the $\nu_{15}(a_g)$ vibration was excited with an intensity comparable to that of the $\nu_2(a_g)$ vibration, it is plausible that the $\nu_{15}(a_g)$ vibration will also be strongly excited in the third electronic transition. The spectrum can now be interpreted on the basis of the following assumptions:

(a) The prominent totally symmetric vibrations are $\nu_2(a_g)$ and $\nu_{15}(a_g)$.

(b) Each transition is split by 350 cm^{-1}. In Table

TABLE XI. Excited state vibrational frequencies as obtained from present work.

Material	State E_{1u}	State B_{1u}	State B_{2u}
Toluene-d_8	···	490[a] $\nu_{18}(a_1)$	456 $\nu_{18}(a_1)$
		$\nu_{18}(b_1)$	520 $\nu_{18}(b_1)$
	940 $\nu_2(a_1)$	950 $\nu_2(a_1)$	920 $\nu_2(a_1)$
m-Xylene	···	520[a] $\nu_{18}(a_1)$	640[b] $\nu_{18}(a_1)$
		$\nu_{18}(b_1)$	$\nu_{18}(b_1)$
	930 $\nu_2(a_1)$	940 $\nu_2(a_1)$	970 $\nu_2(a_1)$
p-Xylene	···	··· $\nu_{18}(a_g)$	360 $\nu_{18}(a_g)$
	···	500 $\nu_{18}(b_{1g})$	540 $\nu_{18}(b_{1g})$
	700 $\nu_2(a_g)$	750 $\nu_2(a_g)$	770 $\nu_2(a_g)$
	1120 $\nu_{15}(a_g)$	1200 $\nu_{15}(a_g)$	1180 $\nu_{15}(a_g)$
	···	1500[c] $\nu_{16}(a_g)$	1570[c] $\nu_{16}(a_g)$
		$\nu_{16}(b_{1g})$	$\nu_{16}(b_{1g})$

[a] The two components are not resolved in the matrix.

[b] The components are assumed by Sponer and Cooper (Ref. 15) to be indistinguishable.

[c] Appears only in overlapping with another combination band.

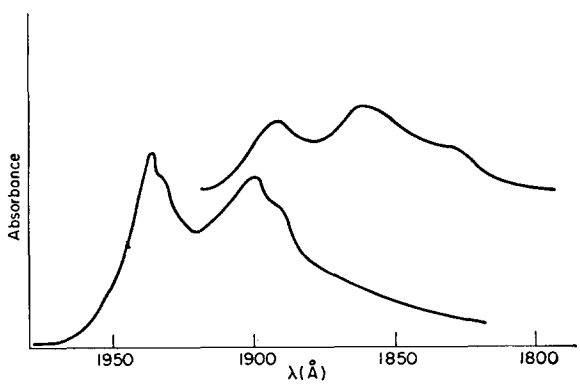

FIG. 6. The 1900-Å absorption system. Upper curve: Toluene-d_8 in krypton matrix, deposition at 40°K and measurement at 20°K. Lower curve: *m*-Xylene in krypton matrix deposition and measurement at 20°K.

TABLE XII. Electronic origins and methyl shifts for $\pi\rightarrow\pi^*$ transitions of methylated benzenes in solid krypton.[a,b]

Molecule	State			
	E_{1u} (Kr)	B_{1u} (Kr)	B_{2u} (Kr)	B_{2u} (gas)
Benzene[b,c,d]	53 810	pe 47 570	pe 37 975	pe 38 089
		fo 48 190	fo 38 505	fo 38 609
Toluene	52 710 (1100)	46 290 (1280)	37 260 (710)	37 477 (610)
o-Xylene	...	...	...	37 308 (781)
m-Xylene	51 600 (2210)	46 230 (1340)	36 710 (1260)	36 955 (1134)
p-Xylene	51 570 (2240)	45 290 (2280)	36 540 (1430)	36 733 (1356)

[a] Data refer to energies in cm^{-1} for the 0–0 line. Data in parenthesis correspond to methyl shift (in cm^{-1}) relative to the 0–0 line in benzene.

[b] (Kr) refers to a krypton matrix at 20°K, while (gas) corresponds to gas-phase data (Refs. 14–16).

[c] Benzene matrix data from Ref. 2.

[d] The first figure in this row for the B_{1u} and B_{2u} states corresponds to the pure electronic origin (pe), while the second number refers to the false origin (fo) induced by the 520-cm^{-1} e_{2g} vibration.

XVI we present the analysis of this transition. In view of the quite appreciable line broadening (linewidth $\sim$250 cm^{-1}) overlap between some components of the spectrum is encountered. In particular, as each of the vibronic bands is split by 350 cm^{-1} overlap occurs between the high-energy component of the $\nu_2(a_g)\simeq$ 740-cm^{-1} vibration and the lower-energy component of the $\nu_{15}(a_g)\simeq$1160-cm^{-1} vibration.

We shall now focus our attention on the nature of the 350-cm^{-1} splitting observed in the third electronic transition by *p*-xylene. Possible assignments are:

(a) Site splitting: The possibility this splitting is due to different trapping sites is excluded on the basis of the expectation that simultaneous appearance of the fine structure (which is assigned to different trapping sites) is expected for all the three $\pi\rightarrow\pi^*$ transitions of the trapped molecule. Although the site splittings differ in energy for different transitions the intensity pattern is expected to be the same. Now, the spectra reported in Figs. 3 and 7 were obtained on the sample sample. The intensity ratio of the different trapping sites in the first transition of *para*-xylene is 50:5:1, whereas in the third transition the intensity ratio of the first two lines separated by 350 cm^{-1} is 1:1.

(b) Simple vibrational assignment: It may be argued that the 0–0+350 cm^{-1} line corresponds to a $\nu_{18}(a_g)$ vibration, as observed for the first transition (see Table V). This possibility is also excluded on the basis of the experimental intensity ratios. The line which is assigned to the $\nu_{18}(a_g)$ vibration in the first transition of *para*-xylene exhibits an extremely weak intensity relative to the 0–0 line (see Table V), and is missing in the second transition of this molecule. From our previous study of the benzene molecule[2] we may assert that the potential energy surfaces (and thus the Franck–Condon factors and the vibrational frequencies) are expected to be similar in all $\pi\rightarrow\pi^*$ states. It is thus unreasonable to expect that the symmetric $\nu_{18}(a_g)$ vibration will be considerably enhanced in the third $\pi\rightarrow\pi^*$ transition so that it will have an intensity comparable to that of the 0–0 line.

As the trivial interpretations can be quite safely excluded, we assign the observed structure in the third electronic transition of *para*-xylene (Table XVI) to the electronic splitting of the $^1A_g\rightarrow{}^1B_{2u}$ and the $^1A_g\rightarrow{}^1B_{3u}$ transitions, which are of the $^1A_{1g}\rightarrow{}^1E_{1u}$ parentage in the benzene molecule.

VII. ELECTRONIC SPLITTING IN THE 1900-Å BAND OF *PARA*-XYLENE

The present work provides experimental evidence for the splitting of the third, spin allowed, nearly degenerate excited state of the *p*-xylene molecule. The assignment of the 0–0 band of the third transition (1850 Å) of *p*-xylene is entirely consistent with the methyl shifts (see Table XVI). In view of the analysis of the experimental data (see Sec. VI), trivial splitting mechanisms can be quite safely excluded. We thus believe that the splitting of 350 cm^{-1} in *p*-xylene corresponds to the removal of

TABLE XIII. Analysis of the absorption spectrum of toluene-h_8 in solid krypton at 20°K; 1900 Å transition ($^1A_{1g}\rightarrow{}^1E_{1u}$ in benzene).

Wavelength (Å)	Frequency (cm^{-1})	Intensity (relative units)	$\nu-\nu_{00}$ (cm^{-1})	Assignment
1897	52 710	2	0	0–0
1865	53 620	3	910	0–0+$\nu_2(a_1)$
~1831	~54 610	1	~1900	0–0+$2\nu_2(a_1)$

TABLE XIV. Analysis of the absorption spectrum of toluene-d_8 in solid krypton; 1900-Å transition ($^1A_{1g}\rightarrow{}^1E_{1u}$ in benzene).

Wavelength (Å)	Frequency (cm^{-1})	Intensity	$\nu-\nu_{00}$ (cm^{-1})	Assignment
1891	52 880	s	0	0–0
1858	53 820	vs	940	0–0+$\nu_2(a_1)$
~1829	~54 680	m	~1800	0–0+$2\nu_2(a_1)$

TABLE XV. Analysis of the absorption spectrum of *m*-xylene in solid krypton at 20°K; 1900-Å transition ($^1A_{1g} \rightarrow {}^1E_{1u}$ in benzene).

Wavelength (Å)	Frequency (cm^{-1})	Intensity	$\nu-\nu_{00}$ (cm^{-1})	Vibrational assignment
1938	51 600	s	0	0–0
1931.4	51 780	Shoulder		0–0+180 cm^{-1}
1904	52 520	s	920	0–0+$\nu_2(a_1)$
1893	52 830	Shoulder		0–0+$\nu_2(a_1)$+310 cm^{-1}
1869	53 460	w	1860	0–0+$2\nu_2(a_1)$
1856	53 880	Shoulder		0–0+$2\nu_2(a_1)$+400 cm^{-1}

degeneracy of the $^1B_{2u}$ and $^1B_{3u}$ states which are of $^1E_{1u}$ parentage in the benzene molecule. It is now well established that the $^1E_{1u}$ $\pi \rightarrow \pi^*$ excited state of the benzene molecule should not exhibit Jahn–Teller coupling effects. However, methyl substitution will lead to the splitting of electronic degeneracy and to vibronic coupling between the zero-order close-lying levels. Hobey's calculations[9] on the ground state of negative ions of substituted benzenes lead to the conclusion that pseudo-Jahn–Teller coupling effects tend to reduce the initial electronic splitting. Thus, for toluene $d=708$ cm^{-1}, while $\Delta E=470$ cm^{-1}; while for *p*-diethylbenzene $d=734$ cm^{-1} and $\Delta E=484$ cm^{-1}. (Here d refers to the initial splitting while ΔE corresponds to the level spacing.) The experimental level splitting in the excited state of *p*-xylene is of the correct order of magnitude. It should be pointed out that we have failed to observe this electronic splitting in other methyl substituted benzenes where line broadening in the third excited state is excessive. Theoretical calculations of pseudo-Jahn–Teller coupling in excited electronic states will be of considerable interest.

VIII. LINE BROADENING

A considerable difference is observed between the linewidths of the first and the higher spin allowed transitions of methylated benzenes in low-temperature krypton matrix. The width of the 0–0 line in the first electronic transition for all the methylated benzenes studied in the present work is about 10–15 cm^{-1}. The higher vibronic components and combination bands are somewhat wider and more diffuse. This width arises from phonon broadening in all the vibronic components and from vibrational relaxation in the excited vibronic manifold (except, of course, for the 0–0 line where the latter effect is absent). In the second electronic transition the width of the 0–0 line is ~250 cm^{-1} for toluene-h_8, ~200 cm^{-1} for toluene-d_8, and ~160 cm^{-1} for *p*-xylene. The higher lines in the second transition in toluene-h_8 and toluene-d_8 are considerably more diffuse, the linewidth exceeding 400 cm^{-1}. For the third transition the linewidths are ~500 cm^{-1} for toluene-h_8 and toluene-d_8 and ~200 cm^{-1} for *p*-xylene. All these data are accurate within ±50 cm^{-1}. Unfortunately, the

TABLE XVI. Analysis of the absorption spectrum of *p*-xylene in solid krypton at 20°K; 1900-Å transition ($^1A_{1g} \rightarrow {}^1E_{1u}$ in benzene).

Wavelength (Å)	Frequency (cm^{-1})	Intensity	$\nu-\nu_{00}$ (cm^{-1})	Vibrational assignment
1939	51 570	vs	0	$[0\text{–}0]_a$
1926	51 920	vs	350	$[0\text{–}0]_b$
1913	52 270	s	700	$[0\text{–}0+\nu_2(a_g)]_a$
1898	52 690	vs	1120	$[0\text{–}0+\nu_2(a_g)]_b$; $[0\text{–}0+\nu_{15}(a_g)]_a$
1883	53 110	s	1540	$[0\text{–}0+2\nu_2(a_g)]_a$; $[0\text{–}0+\nu_{15}(a_g)]_b$
1870	53 480	m	1910	$[0\text{–}0+2\nu_2(a_g)]_b$; $[0\text{–}0+\nu_2(a_g)+\nu_{15}(a_g)]_a$
1855	53 910	w	2340	$[0\text{–}0+3\nu_2(a_g)]_a$; $[0\text{–}0+2\nu_{15}(a_g)]_a$; $[0\text{–}0+\nu_2(a_g)+\nu_{15}(a_g)]_b$
1842	54 290	w–vw	2720	$[0\text{–}0+3\nu_2(a_g)]_b$; $[0\text{–}0+2\nu_{15}(a_g)]_b$; $[0\text{–}0+2\nu_2(a_g)+\nu_{15}(a_g)]_a$
1831	54 620	w–vw	3050	$[0\text{–}0+2\nu_{15}(a_g)+\nu_2(a_g)]_a$; $[0\text{–}0+2\nu_2(a_g)+\nu_{15}(a_g)]_b$
1822	54 880	w–vw	3310	$[0\text{–}0+2\nu_{15}(a_g)+\nu_2(a_g)]_b$
1813	55 160	w–vw	3590	

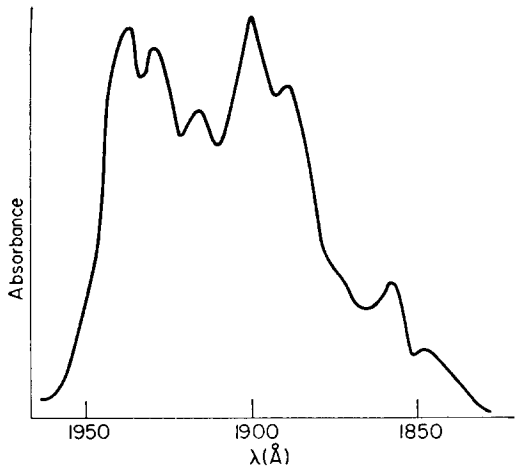

FIG. 7. The 1900-Å absorption system of *p*-xylene in solid krypton. Sample was deposited at 40°K and measured at 20°K.

present data are only semiquantitative as we cannot completely eliminate "trivial effects" such as site splittings. In toluene-h_8 and toluene-d_8 the width of bands of the second and third electronic transition is so large because of overlap of two sites characterized by about equal intensity and a splitting of about 200–300 cm^{-1}. On the other hand, in the second and third electronic transitions of *p*-xylene, the contribution of site splitting has been eliminated to a large extent.

In spite of the inherent limitations of the experimental information we can assess that intramolecular nonradiative decay is extremely efficient in the second and third excited singlet states of methylated benzenes. Two major classes of such processes should be considered: (a) electronic relaxation such as internal conversion and intersystem crossing; (b) photochemical rearrangements and dissociation reactions. From the observed linewidths we can infer that in the second and third excited states of methylated benzenes, the nonradiative decay of these excited states occurs on a time scale shorter than 10^{-14}–10^{-15} sec. Some independent spectroscopic data are consistent with this conclusion. No emission was observed from any alkyl benzene in the gas phase[20] indicating that for the "isolated" molecules the photochemical decay channel dominates electronic relaxation process. Internal conversion in higher excited states of large aromatic hydrocarbons (which follow excitation to the second excited singlet, decay into the vibronic manifold of lower-lying electronic states and then decay radiatively) are characterized by rates[20] of 10^{12} sec^{-1}, so that the branching ratio for photochemical decay relative to internal conversion in methylated benzenes in the gas phase can be 10^{+3}. On the other hand, solvent effects enhance considerably the internal conversion in methyl benzenes in the pure liquid and in hydrocarbon solvents.[20] In this case, photochemical decay and internal conversion are both efficient. The linewidth data scan the whole nonradiative width and we cannot separate the different decay channels of the excited electronic state. However, the appreciable diffuseness of the higher vibronic components of the second transition in toluene in contrast to the above constant linewidth for *p*-xylene is of interest. It is conceivable that photochemical decay channels become more efficient at higher energy above the 0–0 line of the second transition in the former case. Combination of more refined line shape studies and photochemical investigations may be of considerable interest in molecular photochemistry.

ACKNOWLEDGMENTS

We wish to thank Professor S. Leach and Dr. R. Lopez Dalgano for a useful discussion.

[1] For a complete survey see G. Herzberg, *Electronic Spectra of Polyatomic Molecules* (Van Nostrand, Princeton, N.J., 1966), p. 555.
[2] B. Katz, M. Brith, B. Sharf, and J. Jortner, J. Chem. Phys. **52,** 88 (1970).
[3] R. J. Buenker, J. L. Whitten, and J. D. Petke, J. Chem. Phys. **49,** 2261 (1968).
[4] G. R. Hunt and I. G. Ross, J. Mol. Spectry. **9,** 50 (1962).
[5] K. Kimura and S. Nagakura, Mol. Phys. **9,** 117 (1963).
[6] M. Bixon and J. Jortner, J. Chem. Phys. **48,** 715 (1968).
[7] W. J. Potts, Jr., J. Chem. Phys. **23,** 73 (1955).
[8] É. V. Shpol'skii, Usp. Fiz. Nauk. **80,** 255 (1963) [Sov. Phys. Usp. **6,** 411 (1963)].
[9] W. D. Hobey, J. Chem. Phys. **43,** 2187 (1965).
[10] G. Savitsky and D. F. Hornig, J. Chem. Phys. **36,** 2634 (1962).
[11] M. Brith and O. Schnepp, Mol. Phys. **9,** 473 (1965).
[12] G. Herzberg, *Infrared and Raman Spectra* (Van Nostrand, Princeton, N.J., 1945).
[13] K. S. Pitzer and D. W. Scott, J. Am. Chem. Soc. **72,** 803 (1943).
[14] N. Ginsburg, W. W. Robertson, and F. A. Matsen, J. Chem. Phys. **14,** 511 (1946).
[15] C. D. Cooper and H. Sponer, J. Chem. Phys. **20,** 1248 (1952).
[16] C. D. Cooper and M. L. N. Sastri, J. Chem. Phys. **20,** 607 (1952).
[17] Y. Diamant, R. M. Hexter, and O. Schnepp, J. Mol. Spectry. **18,** 158 (1965).
[18] A. C. Albrecht, J. Chem. Phys. **33,** 169 (1960).
[19] J. Petrushka, J. Chem. Phys. **34,** 1120 (1961).
[20] C. L. Braun, S. Kato, and S. Lipsky, J. Chem. Phys. **39,** 1645 (1963).